The Plant Cell, Vol. 30: 347–359, February 2018, www.plantcell.org © 2018 ASPB.

GIF Transcriptional Coregulators Control Root Meristem Homeostasis

María Florencia Ercoli,[a] Antonella Ferela,[a] Juan Manuel Debernardi,[a] Ana Paula Perrone,[a] Ramiro E. Rodriguez,[a,b] and Javier F. Palatnik[a,b,1]

[a] IBR (Instituto de Biología Molecular y Celular de Rosario), CONICET, and Universidad Nacional de Rosario, Rosario 2000, Argentina
[b] Centro de Estudios Interdisciplinarios, Universidad Nacional de Rosario, Rosario 2000, Argentina

ORCID IDs: 0000-0001-5587-6227 (M.F.E.); 0000-0002-5266-3346 (A.F.); 0000-0002-4591-7061 (J.D.); 0000-0003-0952-791X (A.P.P.); 0000-0002-0867-4099 (R.E.R.); 0000-0001-7996-5224 (J.F.P.)

In the root meristem, the quiescent center (QC) is surrounded by stem cells, which in turn generate the different cell types of the root. QC cells rarely divide under normal conditions but can replenish damaged stem cells. In the proximal meristem, the daughters of stem cells, which are referred to as transit-amplifying cells, undergo additional rounds of cell division prior to differentiation. Here, we describe the functions of *GRF-INTERACTING FACTORs* (*GIFs*), including *ANGUSTIFOLIA3* (*AN3*), in *Arabidopsis thaliana* roots. GIFs have been shown to interact with GRF transcription factors and SWI/SNF chromatin remodeling complexes. We found that combinations of *GIF* mutants cause the loss of QC identity. However, despite their QC impairment, *GIF* mutants have a significantly enlarged root meristem with additional lateral root cap layers. We show that the increased expression of *PLETHORA1* (*PLT1*) is at least partially responsible for the large root meristems of *an3* mutants. Furthermore, we found that GIFs are necessary for maintaining the precise expression patterns of key developmental regulators and that AN3 complexes bind directly to the promoter regions of *PLT1* as well as *SCARECROW*. We propose that AN3/GIFs participate in different pathways that control QC organization and the size of the meristem.

INTRODUCTION

The indeterminate growth of the *Arabidopsis thaliana* root is supported by the meristem at the tip of the organ. This root meristem is organized into defined domains. The quiescent center (QC), characterized by the expression of the homeodomain transcription factor gene *WOX5* (Petricka et al., 2012a), is surrounded by stem cells, which in turn are responsible for the different cell types that comprise the stereotypical Arabidopsis root. QC cells barely divide under normal conditions, although their proliferation can be activated after the stem cells are damaged (Cruz-Ramírez et al., 2013; Heyman et al., 2013; Vilarrasa-Blasi et al., 2014). The QC and adjacent stem cells are specified by two parallel routes directed by the transcription factors PLETHORA (PLT) and SHORTROOT (SHR)/SCARECROW (SCR) (Petricka et al., 2012a; Heyman et al., 2014). Shootward from the QC, in the proximal meristem, the stem cell progeny undergoes rapid, transient-amplifying cell divisions that provide the necessary number of cells for organ growth (Scheres, 2007; Heidstra and Sabatini, 2014).

Transcription factors of the GROWTH-REGULATING FACTOR (GRF) class are defined by the presence of a WRC and QLQ domain, which are necessary for DNA binding and protein-protein interactions, respectively. In Arabidopsis roots, the *GRFs* are specifically expressed in transit-amplifying cells located in the proximal meristem, where they promote rapid cell divisions while repressing genes that are active in stem cells (Rodriguez et al., 2015). This precise localization of the GRFs in transit-amplifying cells is accomplished through posttranscriptional repression by the microRNA miR396, which excludes the GRFs from the stem cell region (Rodriguez et al., 2015).

The GRFs interact with small cofactors called GRF-INTERACTING FACTORs (GIFs). In Arabidopsis, the *GIF* family is composed of three members: *ANGUSTIFOLIA3* (*AN3*; also known as *GIF1*), *GIF2*, and *GIF3*, which promote the growth of leaves and aerial organs (Kim and Kende, 2004; Horiguchi et al., 2005). GIFs cannot bind to DNA per se, but they can function as coactivators of the GRFs (Kim and Kende, 2004; Horiguchi et al., 2005; Debernardi et al., 2014; Nelissen et al., 2015; Rodriguez et al., 2016). In addition, AN3 can interact with BRAHMA, a central component of the SWI/SNF chromatin remodeling complexes (Debernardi et al., 2014; Vercruyssen et al., 2014; Nelissen et al., 2015). GIFs are defined by an N-terminal domain that is homologous to the SNH domain present in human SYNOVIAL TRANSLOCATION (SYT) (Kim and Kende, 2004; Horiguchi et al., 2005), which mediates the interaction with human BRAHMA and BRAHMA RELATED GENE1 (Nagai et al., 2001; Perani et al., 2003). Therefore, while the interactions between GIFs/SYT and BRAHMA complexes are conserved between animals and plants, the partnership between GIFs and GRFs has been acquired more recently in evolution, as the GRFs are plant-specific transcription factors.

In the aerial part of the plant, the downregulation of GRF activity through miR396 overexpression or loss-of-function mutants in *AN3* and other *GIFs* have similar effects, including a reduction in meristem and leaf size (Kim and Kende, 2004; Horiguchi et al., 2005; Rodriguez et al., 2010; Lee et al., 2014). Here, we describe the functions of the GIF coregulators in root development and show that they play a broad role in maintaining homeostasis of

[1] Address correspondence to palatnik@ibr-conicet.gov.ar.
The author responsible for distribution of materials integral to the findings presented in this article in accordance with the policy described in the Instructions for Authors (www.plantcell.org) is: Javier F. Palatnik (palatnik@ibr-conicet.gov.ar).
www.plantcell.org/cgi/doi/10.1105/tpc.17.00856

the root meristem. Most conspicuously, GIFs are necessary to maintain the QC, a function that is independent of GRF transcription factors. Surprisingly, *gif* mutants that have a distorted QC also have significantly enlarged root meristems. We propose that GIFs act through different partners, including the GRFs and BRAHMA complexes, to maintain the homeostasis of the root meristem. Furthermore, we show that AN3 complexes directly regulate *PLT1* and *SCR*, highlighting the importance of this system in fine-tuning cellular programs during root development.

RESULTS

Control of the QC by GIF Coregulators

The three members in the Arabidopsis *GIF* family of transcriptional coregulators (Figure 1A) encode polypeptides harboring a SNH and QG domain (Kim and Kende, 2004). We characterized the root tip architecture in individual, double, and triple mutants (Figures 1B and 1C). Single mutants, as well as *an3 gif3* and *gif2 gif3* double mutants, presented a normal cellular organization in the QC (Figures 1B and 1C; Supplemental Figure 1). However, *an3 gif2* and *an3 gif2 gif3* displayed a strong disorganization of the QC (Figures 1C and 1D; Supplemental Figure 1). Unlike the two to three cells that are well defined in size and shape in a longitudinal section of the wild-type QC, we found no regular organization in the presumptive QC region of the *an3 gif2* or *an3 gif2 gif3* mutants (Figures 1C and 1D; Supplemental Figure 1). All *an3 gif2 gif3* triple mutants analyzed and ~70% of *an3 gif2* double mutants displayed a strong distortion of the QC area (Figures 1C and 1D; Supplemental Figure 1). We analyzed the expression of QC marker *ProWOX5:GFP* (Sarkar et al., 2007) by crossing the reporter line to the different mutants and found it to be severely affected in *an3 gif2*, which is in good agreement with the disorganization of the QC (Figures 1E and 1F).

To validate our observation that the distortion of the QC in *an3 gif2* and *an3 gif2 gif3* was caused by reduced GIF activity, we generated a dominant repressor version of AN3 by fusing the EAR-repression motif (SRDX) (Hiratsu et al., 2003) to the C terminus of the protein. Plants harboring *ProAN3:AN3-SRDX*, in which *AN3-SRDX* is expressed under the control of *AN3* regulatory regions, displayed a strong distortion of the QC and a strong reduction in *ProWOX5:GFP* expression in 26 out of 44 transgenic plants analyzed (Figure 1G). Taken together, these results indicate that *GIF* coregulators are necessary to maintain the QC in Arabidopsis roots.

Control of Root Meristem Size by GIF Coregulators

Analysis of primary root growth in *gif2*, *gif3*, and *gif2 gif3* mutants showed no obvious differences compared with wild-type plants (Figures 2A and 2B; Supplemental Figures 2A and 2B). In contrast, *an3* single mutants had longer roots than the wild type, a phenotype that was confirmed in mutants of two different accessions (Figures 2A to 2C; Supplemental Figure 3A). Interestingly, *an3 gif2* double mutants had shorter roots than the wild type (Figures 2A and 2B), and *an3 gif2 gif3* triple mutants were even more affected (Figures 2A to 2C). Next, we determined the root meristem size in the different *GIF* mutants. We found that *an3*, *an3 gif3*, *an3 gif2*, and *an3 gif2 gif3* mutants displayed significantly larger meristems than wild-type plants (Figures 2D and 2F; Supplemental Figures 2 and 3). In all cases, the larger meristem was a consequence of a higher number of meristematic cells (Figure 2G; Supplemental Figures 2D and 3C). Overall, *an3* single mutants had an enlarged root meristem and longer roots than wild-type plants, while *an3 gif2* or *an3 gif2 gif3* mutants, which had larger meristems together with a strong disorganization of the QC, had shorter roots. We estimated the cell cycle duration in the different mutants and found it to be delayed in *an3 gif2 gif3* mutants compared with wild-type roots (Supplemental Figure 4). Next, we overexpressed the three Arabidopsis *GIFs* (i.e., *AN3*, *GIF2*, and *GIF3*) under the control of the *35S* promoter. In all cases, we found that high *GIF* levels caused a reduction in meristem length (Figures 2E and 2H) due to a decrease in cell number (Figure 2I), a phenotype opposite to that observed in *gif* mutants. Altogether, these results indicate that GIFs quantitatively control root meristem size, while a strong downregulation of GIF activity (e.g., combination of mutants or *AN3-SRDX*) impairs the QC.

To investigate whether the effects of the *an3 gif2* mutants in the root meristem were reversible, we generated a *ProAN3:AN3-GR-GFP* (*AN3-GR*) fusion, in which AN3 activation is triggered by dexamethasone (DEX), and introduced it into *an3 gif2* mutants. After 30 h of DEX treatment, the size of the root meristem of the *an3 gif2* mutants harboring *AN3-GR* began to recover and was fully complemented 40 h after DEX treatment (Figures 3A and 3B). Interestingly, 40 h after DEX treatment, the QC organization was recovered in *an3 gif2* mutants harboring *AN3-GR* in most cases (only 15% of *an3 gif2* double mutants showed a strong QC distortion; Supplemental Table 1; Figure 3C). Altogether, these results confirm that the defects observed in the *AN3*/*GIF* mutants were caused by low levels of these transcriptional coregulators and were at least partially reversible upon activation of AN3.

GIF Coregulators and Their Partners Are Expressed in Different Root Domains

Prompted by the observation that the overexpression of *AN3*, *GIF2*, and *GIF3* caused similar phenotypes, but only *an3* single mutants were affected in the root meristem, we decided to analyze their expression patterns in Arabidopsis roots. We generated reporters for the three *GIFs* by fusing *GFP* to the C-terminal part of each gene. We found that *ProAN3:AN3-GFP* (*AN3:GFP*; Figure 4D) was strongly expressed in the root meristem and QC region, while *ProGIF2:GIF2-GFP* (*GIF2:GFP*; Figure 4E) was more broadly expressed, including the elongation zone and columella cells. *ProGIF3:GIF3-GFP* (*GIF3:GFP*) expression was restricted to the vascular region (Figure 4F), indicating that the three genes have overlapping but not identical expression patterns. Of the 40 independent reporter lines analyzed for each gene, these patterns of expression were observed in more than 90% of the lines for *AN3:GFP* (Figure 4D) and *GIF2:GFP* (Figure 4E), and in more than 60% for *GIF3:GFP*, which was detected at lower levels (Figure 4F). In addition, only *AN3* showed a strong peak of expression in the QC and stem cell region (Figure 4D, inset), which is in agreement with previous reports that identify *AN3* as a QC-enriched gene (Nawy et al., 2005), and with the defects in the QC of *an3 gif2* and *an3 gif2 gif3* mutants, but not of *gif2 gif3* (Figures 1C and 1D). Finally, we measured *AN3* and *GIF2* transcript levels in *an3*, *gif2*, and *an3 gif2* mutants (Figures 4B and 4C) and found that *AN3* transcript levels

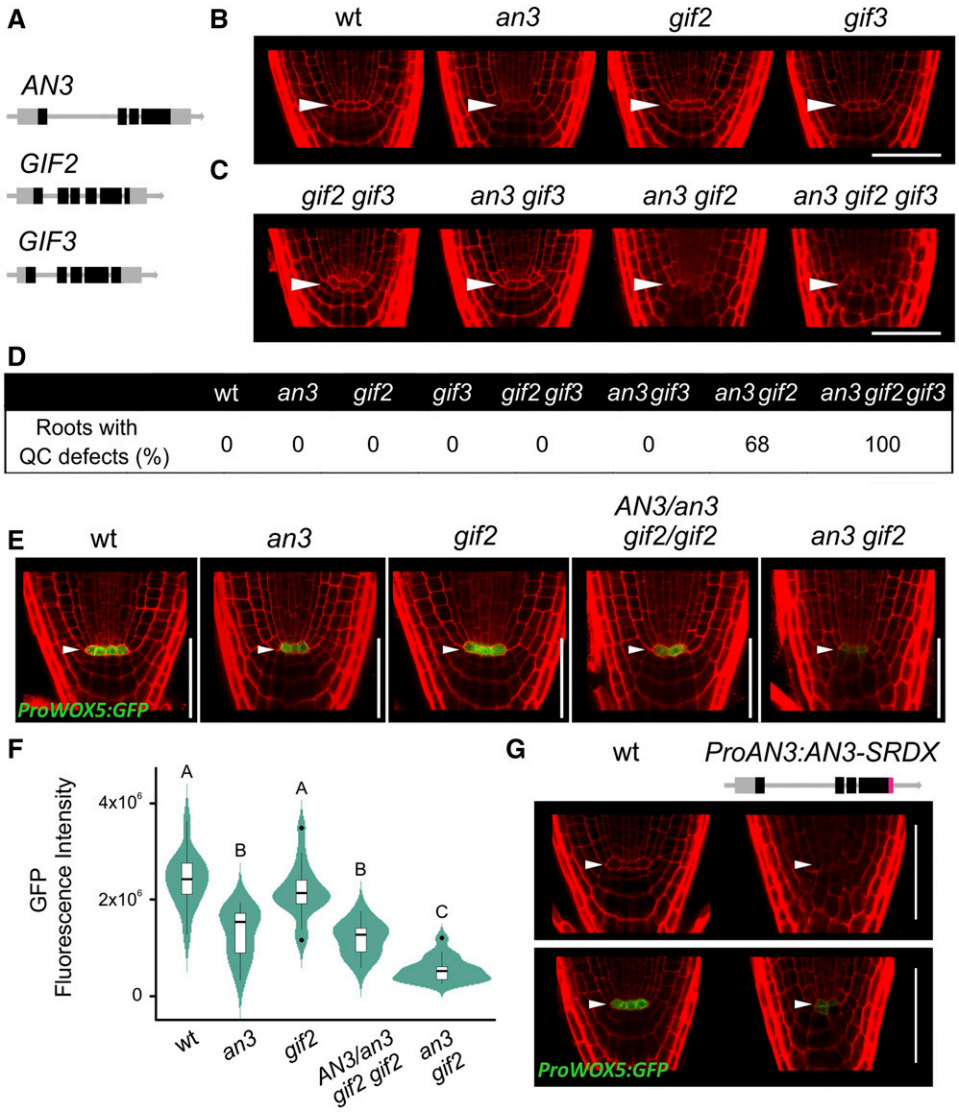

Figure 1. *GIFs* Are Necessary to Maintain the QC.

(A) Schematic comparison of the gene structures of different members of the Arabidopsis GIF family. The light-gray boxes represent the untranslated region, while the dark boxes are the exon sequences.

(B) QC organization in roots of the wild type and single mutants *an3*, *gif2*, and *gif3* at 7 d after sowing. The white arrowheads mark the position of the QC. Bars = 50 μm.

(C) QC organization in roots of multiple *GIF* mutants *gif2 gif3*, *an3 gif3*, *an3 gif2*, and *an3 gif2 gif3* 7 d after sowing. The white arrowheads mark the position of the QC. Bars = 50 μm.

(D) Percentage of roots with strong QC distortion in different mutant backgrounds. Wild-type and *an3 gif2* QC organization was assayed in more than 140 plants. In the other cases, at least 50 roots were evaluated for each background.

(E) Expression of *ProWOX5:GFP* in the wild type, *an3*, *gif2*, *AN3/an3 gif2/gif2*, and *an3 gif2*. The white arrowheads mark the position of the QC. Bars = 50 μm.

(F) Combined box/violin plot diagram of GFP fluorescence intensity from the *ProWOX5:GFP* reporter in the wild-type, *an3*, *gif2*, *AN3/an3 gif2/gif2*, and *an3 gif2* background. Different letters indicate significant differences, as determined by ANOVA followed by Tukey's multiple comparison test ($P < 0.05$). The data show the GFP fluorescent intensity scored in 25 different plants of each genotype. The combined box/violin plot was produced in R using the ggplot2 library with default parameters. Outliers are plotted as individual dots.

(G) QC organization in roots of the wild type transformed with a dominant repressor version of AN3 (*ProAN3:AN3-SRDX*) or an empty vector (wt) at 7d after sowing. Below, the expression of *ProWOX5:GFP* in the wild type and *ProAN3:AN3-SRDX*. The white arrowheads mark the position of the QC. A schematic representation of *ProAN3:AN3-SRDX* is shown (light-gray boxes represent untranslated regions, dark boxes represent exons, and the pink box indicates the SRDX sequence). Bars = 50 μm.

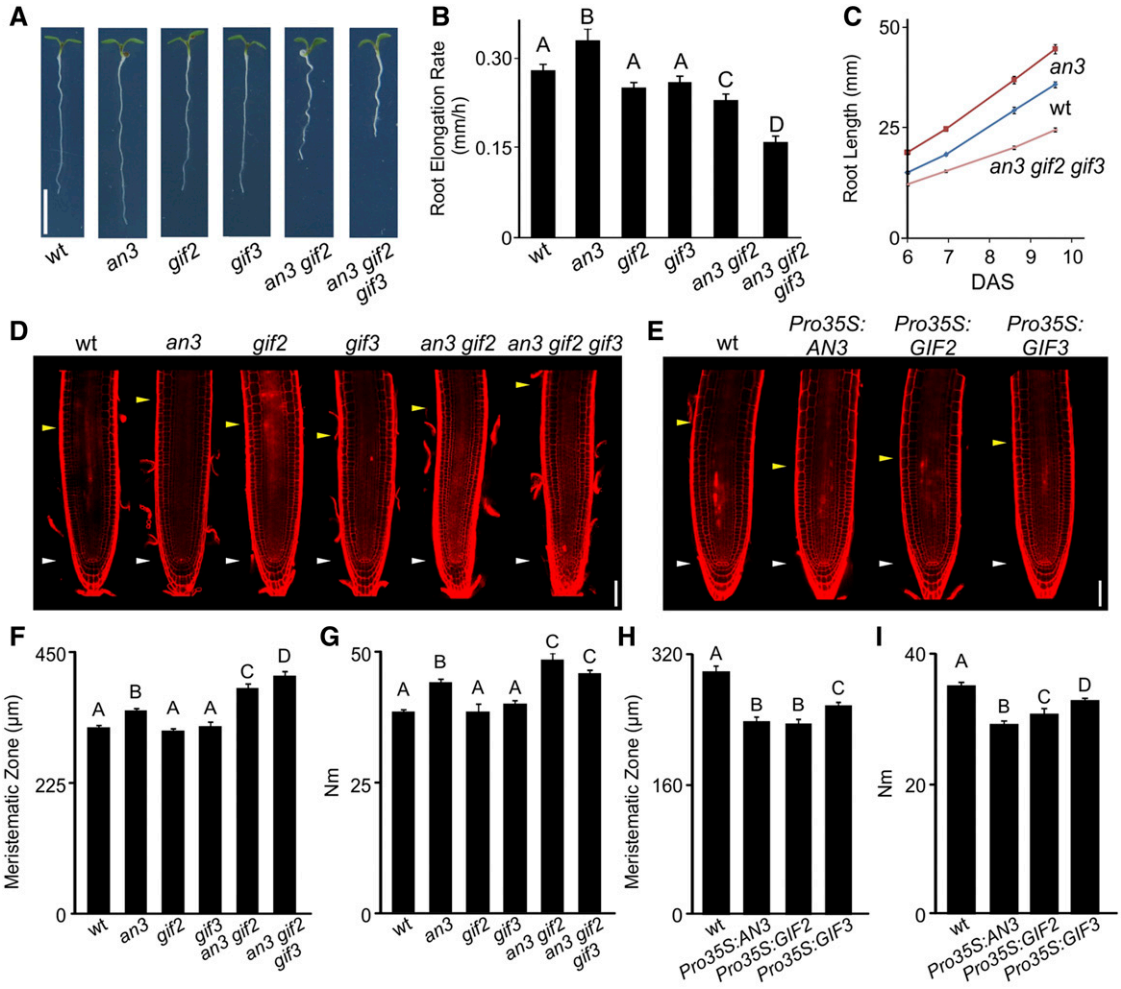

Figure 2. *GIFs* Regulate Root Meristem Size and Growth.

(A) Root growth phenotype 6 d after sowing in the wild type, *an3*, *gif2*, *gif3*, *an3 gif2*, and *an3 gif2 gif3*. Bar = 1 cm.

(B) Root elongation rate (mm/h) in the wild type, *an3*, *gif2*, *gif3*, *an3 gif2*, and *an3 gif2 gif3.* The data shown are mean ± SE of the root elongation rate measured in 25 different roots of each genotype. Different letters indicate significant differences, as determined by ANOVA followed by Tukey's multiple comparison test ($P < 0.05$).

(C) Root elongation (mm) in wild type, *an3* and *an3 gif2 gif3*. DAS (days after sowing). The data shown are mean ± SE of the root elongation over time measured in 25 different roots of each genotype

(D) Root tip architecture 7 d after sowing in the wild type, *an3*, *gif2*, *gif3*, *an3 gif2*, and *an3 gif2 gif3*. The white arrowheads mark the position of the QC, and the yellow arrowheads mark the end of the meristem where cells start to elongate. Bar = 50 µm.

(E) Root tip architecture 7 d after sowing in the wild type, *Pro35S:AN3*, *Pro35S:GIF2*, and *Pro35S:GIF3*. The white arrowheads mark the position of the QC, and the yellow arrowheads mark the end of the meristem where cells start to elongate. Bar = 50 µm.

(F) Meristematic zone length (µm) in the wild type, *an3*, *gif2*, *gif3*, *an3 gif2*, and *an3 gif2 gif3.* The data shown are mean ± SE of the meristematic zone length measured in 25 different roots of each genotype. Different letters indicate significant differences, as determined by ANOVA followed by Tukey's multiple comparison test ($P < 0.05$).

(G) Number of cortex cells in the root meristem (Nm) in the wild type, *an3*, *gif2*, *gif3*, *an3 gif2*, and *an3 gif2 gif3.* The data shown are mean ± SE of the number of meristematic cortex cells scored from 25 different roots of each genotype. Different letters indicate significant differences, as determined by ANOVA followed by Tukey's multiple comparison test ($P < 0.05$).

(H) Meristematic zone length (µm) in the wild type, *Pro35S:AN3*, *Pro35S:GIF2*, and *Pro35S:GIF3.* The data shown are mean ± SE of the meristematic zone length measured in 25 different roots of each genotype. Different letters indicate significant differences, as determined by ANOVA followed by Tukey's multiple comparison test ($P < 0.05$).

(I) Number of cortex cells in the root meristem (Nm) in the wild type, *Pro35S:AN3*, *Pro35S:GIF2*, and *Pro35S:GIF3.* The data shown are mean ± SE of the number of meristematic cortex cells scored from 25 different roots of each genotype. Different letters indicate significant differences, as determined by ANOVA followed by Tukey's multiple comparison test ($P < 0.05$).

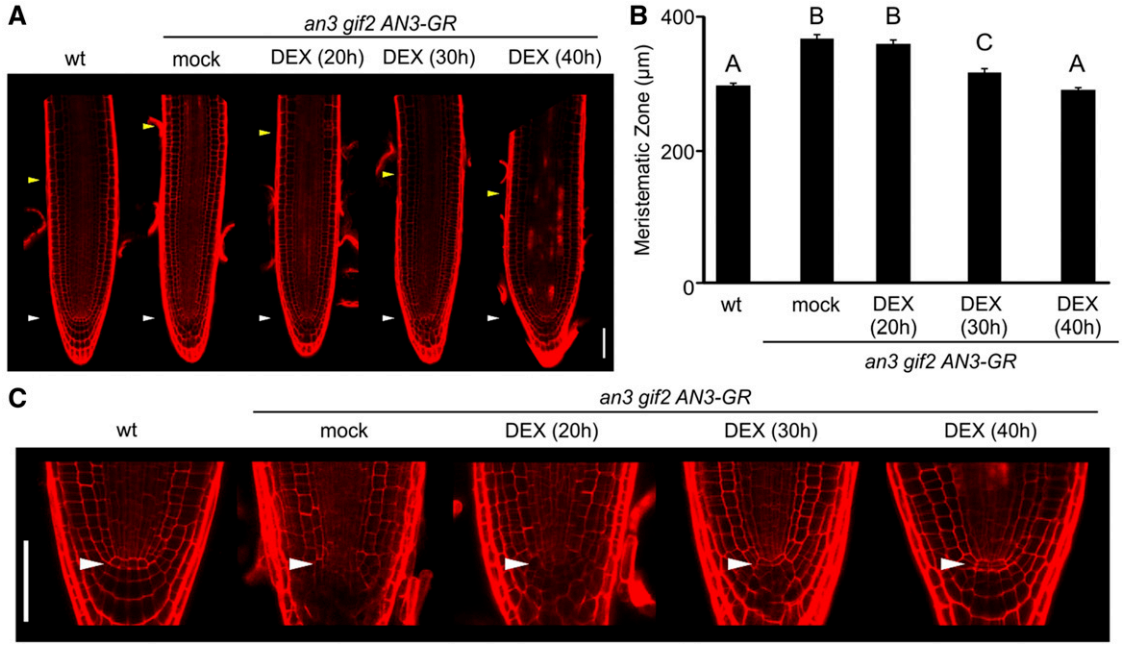

Figure 3. Inducible *AN3-GR* Rescues the Root Meristem Defects in the *an3 gif2* Mutants.

(A) and **(B)** Root meristem size changes in *an3 gif2* mutants harboring *AN3-GR* after DEX treatment.

(A) Root tip architecture at 6 d after sowing in the wild type and *an3 gif2 AN3-GR*. The white arrowheads mark the position of the QC, and the yellow arrowheads mark the end of the meristem where cells start to elongate. Bar = 50 µm.

(B) Meristematic zone length (µm) in the wild type and *an3 gif2 AN3-GR*. The data shown are mean ± SE of the meristematic zone length measured in at least 30 different roots of each genotype. Different letters indicate significant differences, as determined by ANOVA followed by Tukey's multiple comparison test ($P < 0.05$).

(C) QC phenotypes in roots of *an3 gif2* plants harboring *AN3-GR* treated with DEX for 20, 30, and 40 h. See Supplemental Table 1 for a quantification of roots with QC defects upon treatment. Bar = 50 µm.

increased in *gif2* mutants (Figure 4B), suggesting the existence of a compensatory mechanism to maintain GIF activity.

As GIFs are known to interact with GRF transcription factors and BRAHMA complexes (Kim and Kende, 2004; Horiguchi et al., 2005; Debernardi et al., 2014; Vercruyssen et al., 2014; Nelissen et al., 2015) (Figure 4A), we compared the expression patterns of *GRF2*, *GRF3*, and *BRAHMA*, which have been described before (Smaczniak et al., 2012), to those of *AN3*, *GIF2*, and *GIF3*. Both *GRF2* and *GRF3* were specifically expressed in transit-amplifying cells and outside of the stem cell region (Figures 4H and 4I), corresponding to previous results (Rodriguez et al., 2015). In contrast, *BRAHMA* was expressed throughout the meristem, with a peak in the QC-stem cell area, overlapping with the peak of expression of *AN3* (Figure 4G).

The AN3 GRF Pathway Controls Root Meristem Size

We investigated the genetic interactions between *AN3* and its partners. Since the *GRFs* function redundantly (Rodriguez et al., 2015), we analyzed *Pro35S:miR396* plants, which have an overall reduction of GRF activity (Rodriguez et al., 2010, 2015; Ercoli et al., 2016). Previous studies have shown that *Pro35S:miR396* roots have a large meristem that can be rescued via the expression of a miR396-resistant version of *GRF3* (*rGRF3*) that is insensitive to the repression by the microRNA (Rodriguez et al., 2015). We examined 50 independent lines expressing *Pro35S:miR396*. Thirty-six of these lines had a meristem larger than wild-type plants, and 10 of them had a meristem similar to or even larger than *an3 gif2* mutants (Supplemental Figure 5A). That the overexpression of miR396 had a larger effect on root meristem size than *an3 gif2* was not unexpected, as a decrease in the activity of the GRF transcription factors might have a stronger effect than the loss of their co-activators. In agreement with this possibility, it has been shown that *rGRF3* can partially rescue the leaf size defects of *an3* (Debernardi et al., 2014). Despite these large effects on meristem size, *Pro35S:miR396* plants did not show alterations in the QC region (Supplemental Figures 5A and 5B). We then analyzed the effects of overexpression of miR396 in *an3* in 50 independent primary transgenic plants. As previously observed (Rodriguez et al., 2010; Mecchia et al., 2013), we found many plants with defects in the shoot apical meristem, leaf polarity, and size (Figures 5A to 5D). We analyzed the roots of 20 *Pro35S:miR396 an3* plants with strong leaf defects (Figure 5D) and found that the QC was unaffected (Figure 5D). To confirm that *AN3* controls root meristem size through the *GRFs*, we analyzed the effects of *Pro35S:AN3* in plants overexpressing miR396. While *Pro35S:AN3* roots showed a reduction in root meristem size, *Pro35S:miR396* caused the opposite effect (Figures 5E and 5F). Plants harboring both *Pro35S:AN3* and *Pro35S:miR396* obtained by crossing the parental lines had a large root meristem similar to that of *Pro*35S:miR396 plants (Figures 5E and 5F), confirming that AN3 requires the GRFs to modify root meristem size. These results

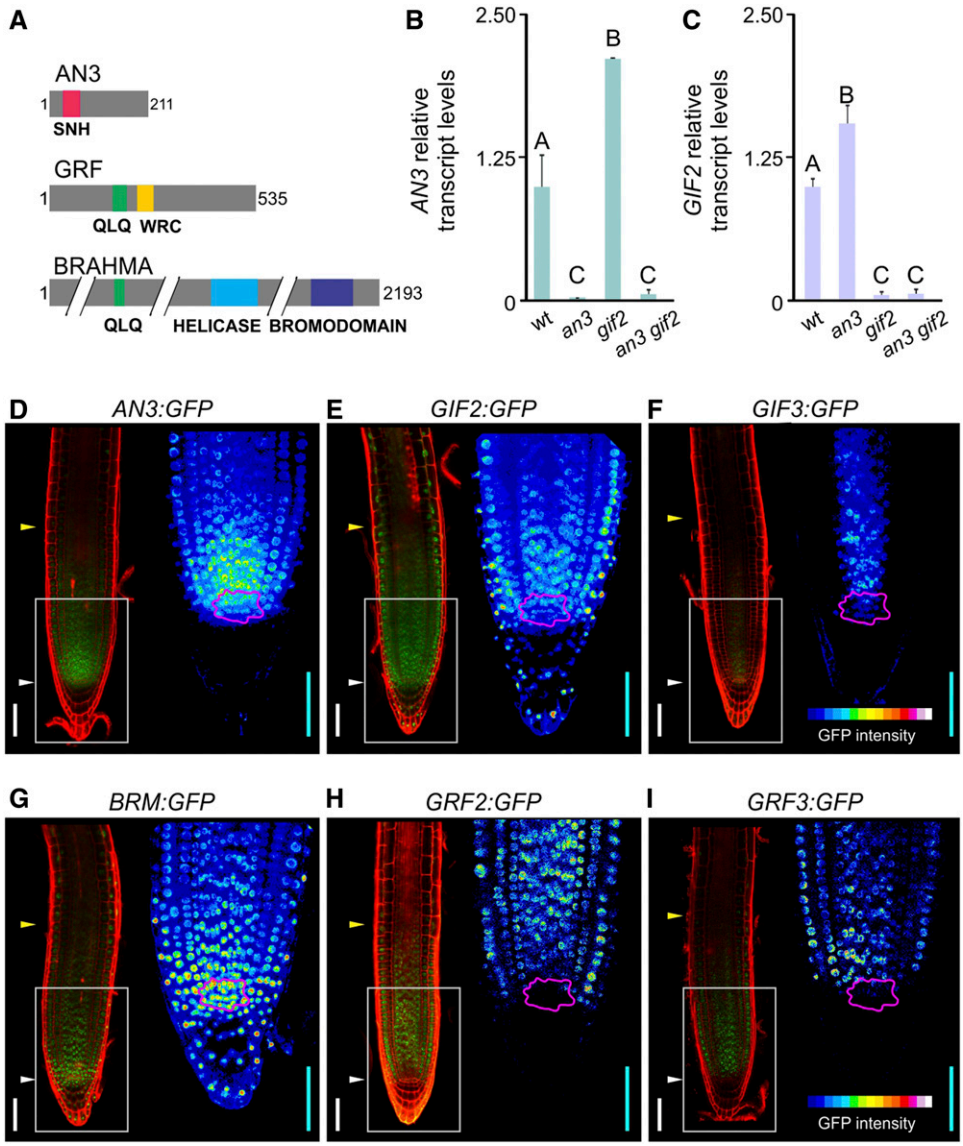

Figure 4. Expression Patterns of *GIF*s, *BRM*, and *GRF*s in the Root Meristem.

(A) Schematic comparison of the domain structures of AN3, a GRF, and BRM.
(B) Relative transcript levels of *AN3* in wild-type, *an3*, *gif2*, and *an3 gif2* roots, as determined by RT-qPCR. The data shown are means ± SE of three biological replicates. Different letters indicate significant differences, as determined by ANOVA followed by Tukey's multiple comparison test ($P < 0.05$).
(C) Transcript level of *GIF2* in wild-type, *an3*, *gif2*, and *an3 gif2* roots, as determined by RT-qPCR. The data shown are means ± SE of three biological replicates. Different letters indicate significant differences, as determined by ANOVA followed by Tukey's multiple comparison test ($P < 0.05$).
(D) to **(I)** Expression of GFP reporters in *AN3* **(D)**, *GIF2* **(E)**, *GIF3* **(F)**, *BRM* **(G)**, *GRF2* **(H)**, and *GRF3* **(I)**. These reporter lines harbor C-terminal translational fusions of GFP to the complete gene, including introns. These constructs are expressed under the control of their own promoter sequences. The figures on the right side of each panel show GFP intensity profile analysis of the regions highlighted with rectangles. Pink shapes indicate the QC and the stem cell region. White and cyan bars = 50 μm.

indicate that AN3 together with the GRFs control root meristem length, but they do not seem to act together to maintain the QC.

Partial Rescue of *brahma* Defects by *an3*

Unlike *Pro35S:miR396* plants, *brahma* mutants have a strong distortion of the QC and a rather short root meristem (Figures 6A, 6B, and 6E) (Yang et al., 2015). We analyzed the genetic interaction between *an3* and *brahma* and found that *an3* restored the root meristem size of *brahma* mutants to a wild-type size (Figures 6A and 6B). As expected, analysis of *an3 brahma* crosses revealed that they also exhibited strong disorganization of the QC area (Figures 6A and 6F). Furthermore, we found that *an3/an3 BRAHMA/brahma* roots had a distorted QC in 77% of the roots

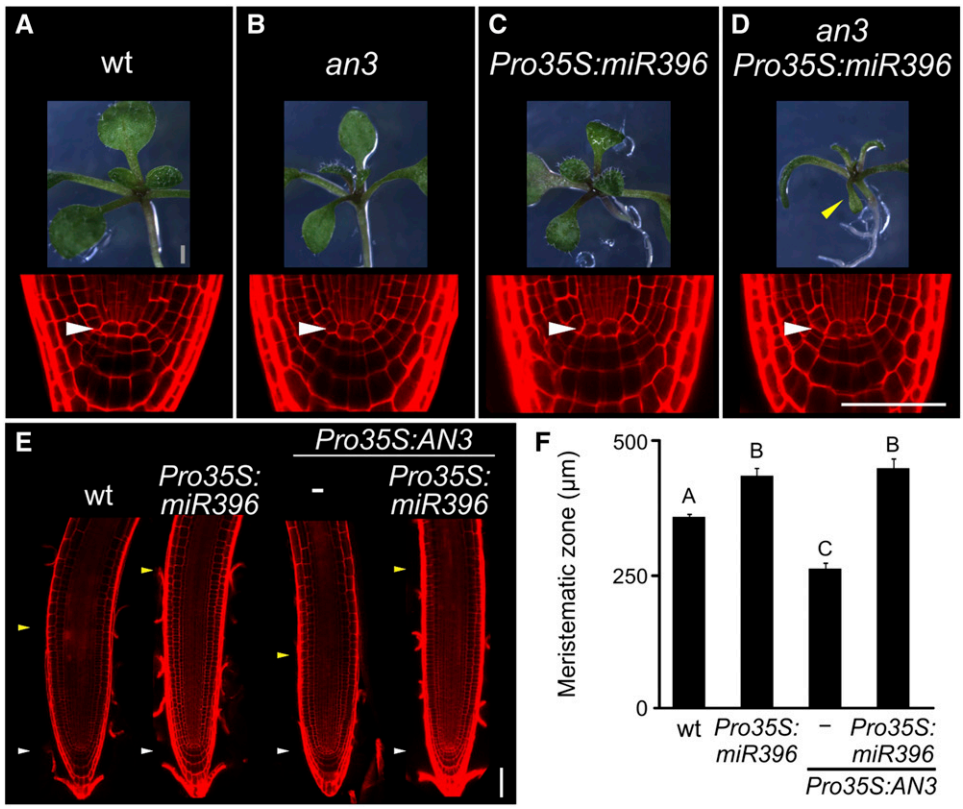

Figure 5. *AN3* Participates in Different Genetic Pathways to Control Specific Zones of the Root Meristem.

(A) to **(D)** Shoot apices (upper figure) and root QC (lower figure) upon overexpression of miR936 in wild-type (S96 accession) and *an3* (*an3-1*) plants. The yellow arrowheads indicate severely affected leaves, while the white arrowheads mark the position of the QC. Gray bar = 1 mm and white bar = 50 μm.
(E) Root meristem size after overexpression of *AN3* driven by the *35S* promoter (*Pro35S:AN3*) in wild-type and miR396-overexpressing plants. The white arrowheads mark the position of the QC, and the yellow arrowheads mark the end of the meristem where cells start to elongate. Bar = 50 μm.
(F) Meristematic zone length (μm) in wild-type, *Pro35S:miR396*, *Pro35S:AN3* (−), and *Pro35S:AN3 Pro35S:miR396* plants. The data shown are mean ± SE of the meristematic zone length measured in 25 different roots of each genotype. Different letters indicate significant differences, as determined by ANOVA followed by Tukey's multiple comparison test ($P < 0.05$).

analyzed (Figures 6A and 6G; Supplemental Table 2), while *an3* or *BRAHMA*/*brahma* did not show QC disorganization per se (Figures 6C and 6D; Supplemental Table 2), indicating that both genes cooperate in maintaining QC homeostasis. Therefore, while *an3* enhanced the QC defects of *brahma*, it partially restored the meristem size. These results are in agreement with the role of *AN3* together with the *GRFs* in the control of the root meristem size and *AN3* together with *BRAHMA* in the maintenance of the QC.

GIFs Fine-Tune Gene Expression in Different Root Domains

To characterize the alterations in the QC and the meristem observed in *an3*/*gif* mutants, we analyzed the expression of cellular markers. We used an *AGL42* reporter (*ProAGL42:GFP*) that is expressed in the QC and the surrounding stele and ground tissue stem cells (Nawy et al., 2005). In *an3*, the activity of the *AGL42* reporter expanded into the transit-amplifying cells (Figures 7A and 7B). A similar effect was previously described in miR396 overexpressors (Figures 7K and 7L). However, in *AN3*/*an3 gif2*/*gif2* and *an3 gif2* double mutants, *AGL42* expression was specifically downregulated in the QC area, while the ectopic expression of this gene in transit-amplifying cells remained active (Figures 7C and 7D; Supplemental Table 3). That only *gif* mutants but not miR396 overexpressors affected *AGL42* expression in the QC is consistent with the notion that *AN3*/*GIFs* functions in QC maintenance independently of the *GRFs*.

We then analyzed the expression of the transcriptional reporters *PLT1* (*ProPLT1:CFP*) and *PLT2* (*ProPLT2:CFP*), which are highly active in the stem cell area and less active in proliferating cells (Galinha et al., 2007; Mähönen et al., 2014). Both the *PLT1* and *PLT2* expression patterns were expanded in *an3* root meristems, although the changes in *PLT1* expression were more obvious (Figure 7F; Supplemental Figure 6). In the *an3 gif2* double mutants, *PLT1* expression decreased in the QC but expanded shootward to a broader area (Figures 7F to 7H), which is consistent with the observed distortion of the QC region and the enlarged proximal meristem. As a consequence, the well-defined gradient of *ProPLT1:CFP* expression along the longitudinal axis was blurred to a larger domain, with rather homogenous expression levels (Figure 7I). Interestingly, an expansion of the expression pattern

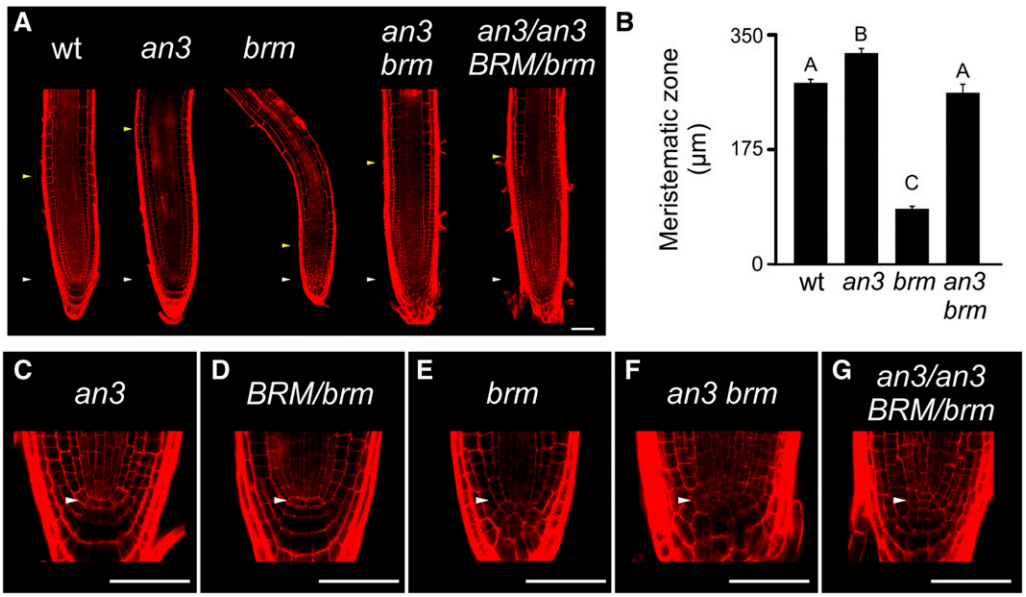

Figure 6. Control of the Root Meristem and QC by AN3 and BRAHMA.

(A) Root tip architecture at 7 d after sowing in the wild type, *an3*, *brm* (*brm-1*), *an3 brm*, and *an3/an3 BRM/brm.* The white arrowheads mark the position of the QC, and the yellow arrowheads mark the end of the meristem where cells start to elongate. Bar = 50 μm.

(B) Meristematic zone length (μm) in the wild type, *an3*, *brm*, and *an3 brm.* The data shown are mean ± SE of the meristematic zone length measured in 25 different roots of each genotype. Different letters indicate significant differences as determined by ANOVA followed by Tukey's multiple comparison test ($P < 0.05$).

(C) to **(G)** QC organization of roots 7 d after sowing in *an3* **(C)**, *BRM/brm* **(D)**, *brm* **(E)**, *an3 brm* **(F)**, and *an3/ an3 BRM/brm* **(G)**. The white arrowheads mark the position of the QC. See Supplemental Table 2 for a detailed analysis of the frequency of roots with QC defects for these genotypes. Bar = 50 μm.

of *ProPLT1:CFP* in transit-amplifying cells was also observed in *Pro35S:miR396* plants. However, in that case, *PLT1* expression was unaffected in the QC (Figures 7J, 7M, and 7N). These results support the notion that *GRFs* and *AN3/GIFs* play a role in the regulation of meristem size and that *AN3/GIFs* have additional functions in the maintenance of the QC. Altogether, our findings show that AN3/GIFs help generate the specific gene expression patterns in the different root domains.

Mechanistic Links between AN3 and the Major Root Regulators *PLT* and *SCR*

Obtaining a readout of the *PLT* gradient is essential for determining the root domains, as the peak of *PLT* expression determines the stem cell niche, while lower levels are necessary to promote cell proliferation in the root meristem (Galinha et al., 2007; Mähönen et al., 2014). We then performed a more detailed analysis of the genetic interaction between *AN3* and *PLT1*, whose expression is significantly affected in *an3/gif* mutants (Figures 7F and 7I). In contrast to *an3*, which has a larger meristem, the loss of *PLT1* led to a reduction in root meristem size (Figures 8A and 8C). Analysis of *an3 plt1* revealed a meristem size identical to that of *plt1*, suggesting that the larger meristem size observed in the *an3* mutants depends on the misregulation of *PLT1* expression (Figures 8A and 8C). As the ectopic expression of *PLT* is associated with an increase in the number of lateral root cap (LRC) layers (Galinha et al., 2007), we analyzed *an3* and *an3 gif2* mutants and found that their roots showed this phenotype (Figures 8B and 8D), which was confirmed by examining the expression of a *SOMBRERO* reporter (*ProSMB:GFP*) (Fendrych et al., 2014). Interestingly, the number of LRC layers in the *an3 plt1* double mutants was similar to that in wild-type roots (Figure 8E), further indicating the importance of *PLT1* misregulation in the developmental defects in *an3* roots.

As *PLT1* was misexpressed in the *an3/gif* mutants (Figures 7F to 7I), we hypothesized that AN3 might be a regulator of *PLT1*. To test this hypothesis, we measured *PLT1* transcript levels in *an3* and found that this gene was upregulated in the root meristem (Figure 8G). We then turned to the DEX-inducible *an3 AN3-GR* system and studied the response of *PLT1* 2 h after *AN3* induction with DEX. We found that *PLT1* transcript levels were significantly repressed upon *AN3* induction (Figure 8H). To confirm that *PLT1* is directly regulated by AN3 complexes, we performed chromatin immunoprecipitation (ChIP) assays using *an3 AN3-GR*-expressing lines. Analysis of the *PLT1* promoter region identified a potential GRF binding site, TGTCAGA (O'Malley et al., 2016), ~4 kb upstream of the coding sequence. We designed primers matching flanking regions of this site, as well as a control region in the *PLT1* coding sequence (Figure 8I). ChIP experiments performed 30 min after DEX treatment of *an3 AN3-GR* with primers designed against *PLT1* promoter regions revealed a strong enrichment, in contrast to the control region (Figure 8I), demonstrating that AN3 complexes can directly bind to the *PLT1* promoter regions and regulate the expression of this gene. In turn, previous studies have shown that *AN3*

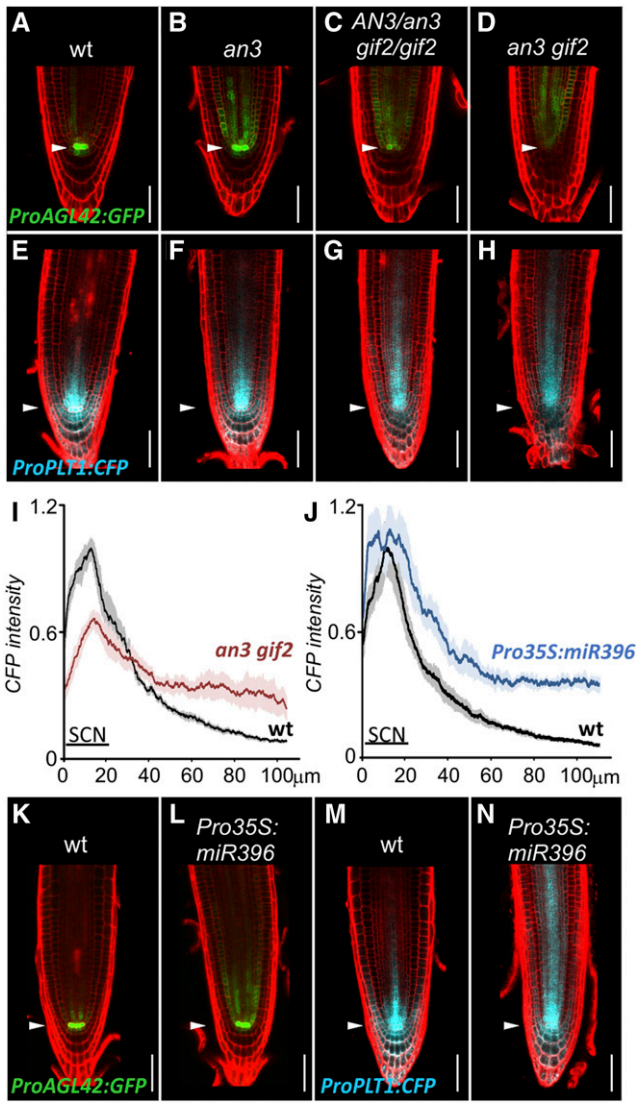

Figure 7. Definition of the Root Developmental Domains by GIFs.

(A) to **(H)** Expression of the reporters *ProAGL242:GFP* (**[A]** to **[D]**) and *ProPLT1:CFP* (**[E]** to **[H]**) in the wild-type (**[A]** and **[E]**), *an3* (**[B]** and **[F]**), *AN3/an3 gif2/gif2* (**[C]** and **[G]**), and *an3 gif2* background (**[D]** and **[H]**). The white arrowheads mark the position of the QC. See Supplemental Table 3 for a detailed analysis of the expression of the reporter *ProAGL42:GFP* in these mutants. Bars = 50 μm.

(I) and **(J)** Profile of fluorescence intensity in root tips of the *ProPLT1:CFP* reporter in the wild type, *an3 gif2* **(I)**, and *Pro35S:miR396* **(J)** roots. The value of CFP intensity was normalized to the maximum value measured in the wild type. The intensity profile corresponds to the average of 10 plants per genotype.

(K) to **(N)** Expression of marker lines *ProAGL242:GFP* (**[K]** and **[L]**) and *ProPLT1:CFP* (**[M]** and **[N]**) in the wild type (**[K]** and **[M]**) and *Pro35S:miR396* background (**[L]** and **[N]**).

is among the genes directly regulated by PLT2 (Santuari et al., 2016). We therefore crossed an *AN3:GFP* reporter line to the *plt1 plt2* mutant and confirmed that *AN3* was significantly downregulated in the progeny (Figure 8F). These results indicate that AN3 and PLT mutually regulate each other.

To explore the additional functions of *AN3* in the QC region, we analyzed the results of a previously described AN3 ChIP-seq experiment performed in Arabidopsis suspension cell cultures (Vercruyssen et al., 2014). Among the 2836 peaks identified in the Arabidopsis genome, we found a potential binding site for an AN3 complex in the *SCR* promoter. We designed primers flanking this putative binding site and confirmed the binding of the AN3 complex to this region by ChIP-PCR using *an3 AN3-GR* plants treated with or without DEX (Figure 8I). Next, we determined the transcript levels of *SCR* after treating *an3 AN3-GR* lines with DEX (Figure 8J) and found an increase in *SCR* levels, further confirming the regulation of *SCR* by AN3. Finally, we expressed the repressor version of AN3, *ProAN3:AN3-SRDX*, in *ProSCR:SCR-GFP* reporter lines. Of the 40 independent transgenic lines analyzed, 22 had a decrease in *SCR-GFP* signal in the QC area (Figure 8K). Altogether, these results indicate that there is a link between AN3 and SCR.

DISCUSSION

The cellular organization of the root meristem is essential for establishing the radial patterning of the root and promoting root growth. Two main pathways, which are directed by SHR/SCR and PLT transcription factors, have been shown to play essential roles in root meristem organization. Mutations in these transcription factors affect the QC and the surrounding stem cells, reduce meristem size, and impair root growth (reviewed in Petricka et al., 2012b; Heyman et al., 2014). Here, we describe the functions of GIF coregulators in root meristem homeostasis. In contrast to other regulators of the root meristem that affect the QC and reduce meristem size (Sabatini et al., 2003; Aida et al., 2004; Ortega-Martínez et al., 2007; Vanstraelen et al., 2009; Chen et al., 2011; González-García et al., 2011; Sang et al., 2012; Moubayidin et al., 2013), the loss of *GIF* genes affects the QC area but increases the size of the meristem.

Expression of GIF Coregulators in Arabidopsis Roots

AN3, *GIF2*, and *GIF3* have overlapping expression patterns, which likely explains their redundant functions. While *GIF2* is expressed rather homogenously throughout the root meristem, *GIF3* expression is enriched in the vascular region. *AN3* has a peak of expression in the stem cell region, with a gradient extending toward the transit amplifying cells. That *AN3* is expressed at higher levels in the stem cell area explains why its mutation affects *WOX5* expression and QC maintenance, especially in combination with other *GIFs*. Interestingly, the pattern of AN3 expression is reminiscent of the gradient of PLT transcription factors (Aida et al., 2004; Galinha et al., 2007; Mähönen et al., 2014). The gene network controlled by PLTs has recently been studied in detail, and *AN3* was consistently detected as a PLT target gene (Santuari et al., 2016). Furthermore, our results showing that overall *AN3* expression was significantly reduced in *plt1 plt2* confirm the biological relevance of this regulation (Figure 8F).

Mechanistic Links between AN3 and Major Root Regulators

In turn, we found that *PLT1* and *PLT2* expression was misregulated in *an3/gif* mutants. The precise expression pattern of *PLT1*, with a peak

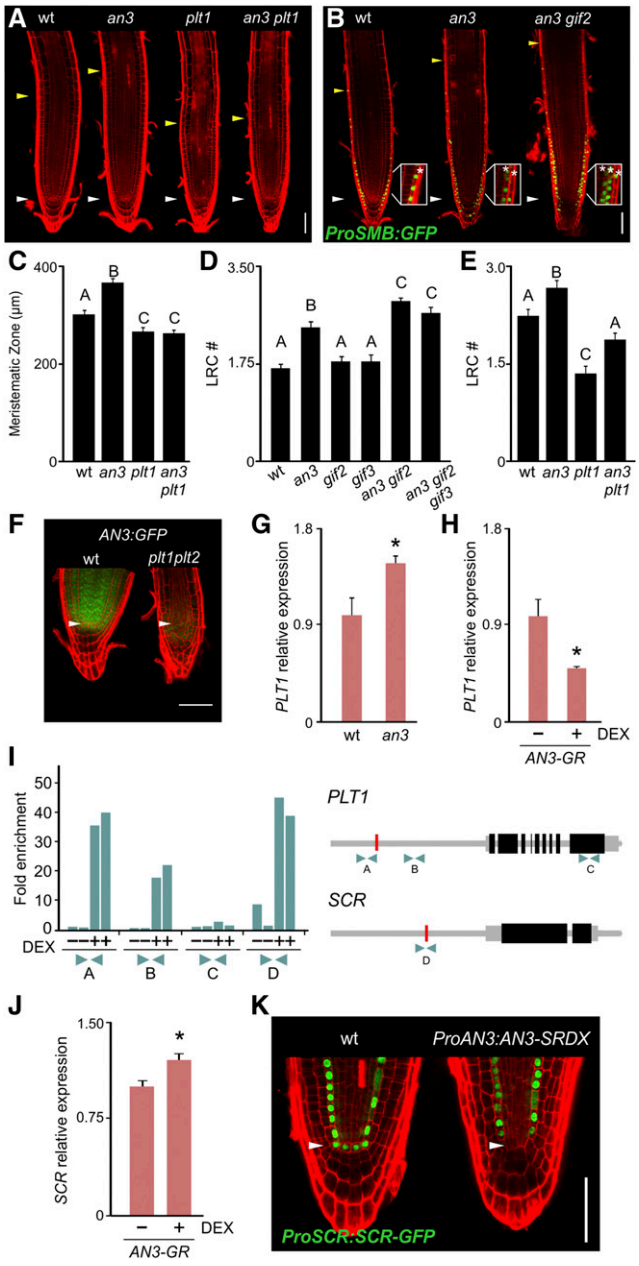

Figure 8. Direct Regulation of *PLT1* and *SCR* by AN3 Complexes.

(A) Root tip architecture 7 d after sowing in the wild type, *an3*, *plt1*, and *an3 plt1*. The white arrowheads mark the position of the QC, and the yellow arrowheads mark the end of the meristem where cells start to elongate. Bar = 50 μm.

(B) Expression of an LRC-specific marker (*ProSMB:GFP*) in wild-type, *an3*, and *an3 gif2* roots. The white arrowheads mark the position of the QC, and the yellow arrowheads mark the end of the meristem where cells start to elongate. The inset magnifies the same position in each root showing the increase in the number of LRC layers. The white stars mark the LRC layers. Bar = 50 μm.

(C) Meristematic zone length (μm) in the wild type, *an3*, *plt1*, and *an3 plt1*. The data shown are mean ± SE of the meristematic zone length measured in 25 different roots of each genotype. Different letters indicate significant differences, as determined by ANOVA followed by Tukey's multiple comparison test ($P < 0.05$).

in the stem cell area that extended toward the proximal meristem, became blurred in the *an3 gif2* double mutant. While the peak of expression of *PLT1* in the stem cell area was reduced in this mutant, its domain of expression extended shootward. The large meristem and ectopic lateral root layers observed in *an3* mutant are consistent with phenotypes caused by the ectopic expression of *PLT* genes (Galinha et al., 2007). The finding that *an3 plt1* crosses suppressed the *an3* phenotypes corroborates the notion that ectopic *PLT1* expression was responsible for these defects. Actually, our *AN3-GR* ChIP PCR analysis showed that AN3 complexes bind directly to the *PLT1* promoter, providing a mechanistic link between AN3 and *PLT* genes. In this context, *AN3/GIFs* coregulators and *PLTs* might be regulating each other's expression to fine-tune their expression patterns. Mutations in *an3/gif* compromise the expression of other genes in the QC such as *WOX5* and *AGL42*. At least *AGL42* expression was upregulated in the meristem, suggesting that AN3/GIF coregulators are necessary for the homeostasis of the root meristem. In addition, we found that AN3 complexes can bind to the *SCR* promoter to regulate its expression. Therefore, AN3 can fine-tune the expression of two genes encoding major regulators

(D) Number of LRC layers measured 35 μm above the QC in the wild type, *an3*, *gif2*, *gif3*, *an3 gif2*, and *an3 gif2 gif3*. The data shown are means ± SE of the number of lateral root cap measured in 25 different roots of each genotype. Different letters indicate significant differences, as determined by ANOVA followed by Tukey's multiple comparison test ($P < 0.05$).

(E) Number of LRC layers measured 35 μm above the QC in the wild type, *an3*, *plt1*, and *an3 plt1*. The data shown are means ± SE of the number of lateral root cap measured in 25 different roots of each genotype. Different letters indicate significant differences, as determined by ANOVA followed by Tukey's multiple comparison test ($P < 0.05$).

(F) Expression of *AN3:GFP* in wild-type (Wassilewskija accession) and *plt1 plt2* mutants. The white arrowheads mark the position of the QC. Bars = 50 μm.

(G) Relative transcript level of *PLT1* in wild-type and *an3* roots, as determined by RT-qPCR. The data shown are means ± SE of three biological replicates. Asterisks indicate significant differences from the wild type, as determined by Student's *t* test ($P < 0.05$).

(H) Relative transcript level of *PLT1* in *an3 AN3-GR* roots after 2 h of DEX induction (+DEX; 25 μM), as determined by RT-qPCR. The data shown are means ± SE of three biological replicates. Asterisks indicate significant differences from mock-treated plants (− DEX), as determined by Student's *t* test ($P < 0.05$).

(I) ChIP-qPCR (left) for three specific regions in the *PLT1* gene named A, B, and C and one specific region in the *SCR* gene named D. The data shown are from two biological replicates. ChIP assays were performed using anti-GFP antibodies on 6-d-old *an3* roots expressing GFP-tagged AN3-GR vector treated with DEX or mock. Right, scheme of AN3 target genes, *PLT1* and *SCR*. A GRF binding site in the *PLT1* promoter and an AN3-complex binding site in the SCR promoter are indicated with red rectangles. The green arrowheads show the position of the primers used in the ChIP-qPCR experiment.

(J) Relative transcript level of *SCR* in *an3 x AN3-GR* roots after 2 h of DEX induction (+ DEX; 25 μM), as determined by RT-qPCR. The data shown are mean ± SE of three biological replicates. Asterisks indicate significant differences from mock-treated plants, as determined by Student's *t* test ($P < 0.05$).

(K) Expression of *ProSCR:SCR-GFP* in wild type (accession Wassilewskija) and plants transformed with a dominant repressor version of AN3 (*ProAN3:AN3-SRDX*) 7 d after sowing. The white arrowheads mark the position of the QC. Bars = 50 μm.

of root development, the PLT and SCR transcription factors. AN3 is then required for the expression of *SCR* in the QC area, while it represses *PLT1* in proliferating cells.

Functions of AN3 and GIF2/3 in Leaves and Roots

Loss of function of *AN3* reduces leaf size (Kim and Kende, 2004; Horiguchi et al., 2005), while additional mutations in *GIF2* and *GIF3* significantly impair leaf growth and the shoot apical meristem (Kim and Kende, 2004; Horiguchi et al., 2005; Lee et al., 2014). Furthermore, simultaneous mutations of *AN3* and *HANABA TANARU* lead to ectopic root formation in cotyledons (Kanei et al., 2012), highlighting the role of the GIF coregulators in the control of shoot development. However, their functions in the above- or belowground parts of the plant appear to differ. In the aerial parts, miR396 overexpressors and *grf* mutants have similar phenotypes to *an3/gif* mutants. Furthermore, *an3 Pro35S:miR396* plants have an affected shoot apical meristem and develop leaves with polarity defects (Rodriguez et al., 2010; Mecchia et al., 2013). In contrast, *Pro35S:miR396* only affects the size of the root meristem without affecting the QC, and *an3 Pro35S:miR396* plants, which have severely affected shoot development, have roots with large meristems (our data). These results suggest that AN3/GIFs have additional functions in roots, especially in QC maintenance, that go beyond the activities of the GRFs.

Control of the QC Region by AN3 and GIF2/3

Detailed studies have shown that AN3 can interact with GRFs (Kim and Kende, 2004; Horiguchi et al., 2005) and BRAHMA chromatin remodeling complexes (Kim and Kende, 2004; Debernardi et al., 2014; Vercruyssen et al., 2014; Nelissen et al., 2015). Furthermore, AN3 is thought to represent a link between the GRFs (or other transcription factors) and chromatin remodeling complexes during leaf development (Vercruyssen et al., 2014; Nelissen et al., 2015). BRAHMA complexes, in turn, are important for the organization of the QC and for modifying the expression of members of the PIN auxin efflux protein family (Yang et al., 2015).

Previous studies have shown that miR396 overexpression does not affect the organization of the QC or *SCR* expression levels (Rodriguez et al., 2015). Here, we showed that AN3 complexes regulate *SCR*, which is required to maintain the QC and stem cells. It is likely that AN3 interacts with BRAHMA to maintain the QC region, but it is plausible that a BRAHMA-AN3 complex also interacts with other transcription factors. It has been proposed that the composition of AN3 complexes dynamically changes along a developing maize (*Zea mays*) leaf (Nelissen et al., 2015), and a similar process might occur in roots as well. Recent studies have described in detail the regulation of cell-specific functions through different protein complexes involving SHORTROOT, SCR, and JACKDAW (Long et al., 2017). We speculate that different AN3 complexes could also be involved in fine-tuning cellular programs in different domains of the root meristem.

METHODS

Plant Materials and Growth Conditions

Arabidopsis thaliana accession Col-0 was used throughout this study unless otherwise indicated. See Supplemental Table 4 for a list and description of the mutants and reporter lines used in this study. Plants were grown in long photoperiods (16 h light/8 h dark) using fluorescent bulbs (triphosphor code #840, 100 μmol quanta m^{-2} s^{-1}) at 21°C. For root analysis, surface-sterilized seeds were sown on solid medium containing 1× Murashige and Skoog salt mixture, 1% sucrose, and 2.3 mM MES (pH 5.8) in 1% agar. After stratifying the seeds in the dark (4°C) for 2 to 3 d, the Petri dishes were placed in a vertical orientation inside growing chambers. For chemical treatments, DEX (D4902-1G; Sigma-Aldrich) was stored as 25 mM stocks in ethanol and used at 25 μM for the indicated periods (2 h and from 20 to 40 h).

Cloning and Generation of Transgenic Lines

See Supplemental Table 5 for a detailed description of the constructs used in this study. For the analysis of expression pattern of *AN3*, *GIF2*, and *GIF3*, the reporter lines were generated by fusing GFP to the C terminus of each protein. A DNA fragment consisting of the promoter region and the genomic sequences (including introns) was used in each case. The *ProAN3:AN3-SRDX* and *ProAN3:AN3-GFP-GR* constructs were obtained in a similar way by fusing the SRDX repression domain or the glucocorticoid receptor coding sequence, respectively, to the C terminus. Arabidopsis plants were transformed using the floral dip method (Clough and Bent, 1998).

Confocal Microscopy

Confocal laser scanning microscopy was performed throughout the study using a Plan Apochromat 20×, 0.8-NA lens on a Zeiss LSM880 microscope. Roots were stained with 10 μg/mL propidium iodide for 2 min, rinsed, mounted in water, and visualized after excitation by an argon 488-nm laser line. The fluorescence emission was collected from 590 to 700nm (propidium iodide), 496 to 542nm (GFP), and 465 to 570nm (CFP). Cellular parameters and fluorescence signal intensity were analyzed with Fiji (Schindelin et al., 2012).

Analysis of Root Growth

For root elongation measurements, seedlings were grown vertically for 10 days. Starting from day 6 after germination until the end of the experiment, a dot was drawn at the position of the root tip. Finally, plates were photographed, and the root length was measured over time with Fiji (Schindelin et al., 2012). Root growth rate, expressed in mm/h, was estimated from the slope of the graph plots of root length (mm) versus plant age (expressed as days after sowing).

Meristematic zone length and meristematic cell number were determined according to the file of cortex cells from the confocal microscopy images. The meristematic zone was defined as the region of isodiametric cells from the QC up to the cell that was twice the length of the immediately preceding cell (Dello Ioio et al., 2008; Long et al., 2017). The average duration of the cell cycle (T) for meristematic cortex cells was calculated as described previously (Rodriguez et al., 2015). For each individual root, the following equation was utilized: $T = (ln2.Nm.Le)\ V - 1$, where *Nm* is the number of meristematic cells in one file of the cortex, *Le* is the average length of fully elongated cortex cells expressed in nm, and *V* is the root growth rate calculated as described previously in mm/h. ANOVA results are provided in Supplemental Table 6.

Gene Expression Analysis via RT-qPCR

Total RNA was isolated from root tissue using Tripure isolation reagent (Roche). Approximately 100 root tips (~2 mm) were collected from each sample at 6 DAG. The numbers of biological replicates, together with the treatment applied, are stated in the corresponding figure legends. Total RNA (0.5 μg) was treated with RQ1 RNase-free DNase (Promega). First-strand

cDNA synthesis was performed using SuperScript III Reverse Transcriptase (Invitrogen). PCR was performed in a Mastercycler ep realplex thermal cycler (Eppendorf) using SYBR Green I (Roche) to monitor double-stranded DNA synthesis. The relative transcript level was determined for each sample and normalized using the *PROTEIN PHOSPHATASE2A* cDNA level (Czechowski et al., 2005). The normalization was performed as described previously (Livak and Schmittgen, 2001). Melting curve analyses at the end of the process and "no template controls" were performed to ensure product-specific amplification without primer-dimer artifacts. Primer sequences are given in Supplemental Table 7.

ChIP

ChIP experiments were performed as described by Kaufmann et al. (2010) with some modifications. The *an3 AN3-GR-GFP* assay was performed using root tips of 6-d-old seedlings using anti-GFP antibody (ChIP Grade; Abcam ab290, lot GR76757-1). Briefly, the seedlings were transferred to plates containing mock medium (DEX −) or medium supplemented with DEX (DEX +) (D4902-1G; Sigma-Aldrich) by lifting the nylon mesh holding the roots with forceps. After 30 min of treatment, the roots were collected (~1500 root tips per sample). Following fixation in 1% (v/v) formaldehyde, the tissues were homogenized and the nuclei isolated and lysed. Cross-linked chromatin was sonicated using a Bioruptor UCD-200 (Diagenode) water bath (15 s on/45 s off pulses; three times). The complexes were immunoprecipitated with 1 μL antibody for 1 h at 4°C with gentle shaking, followed by incubation for 50 min at 4°C with 50 mL of Protein A agarose beads (Invitrogen). Immunoprecipitated DNA was then recovered and analyzed by qPCR. An aliquot of untreated sonicated chromatin was processed in parallel as the total input DNA control. Fold enrichment was calculated with or without the addition of DEX for the indicated regions. The primers used in the ChIP experiments are listed in Supplemental Table 7.

Accession Numbers

Accession numbers (Arabidopsis Genome Initiative locus identifiers) for the genes described in this article are provided in Supplemental Table 7.

Supplemental Data

Supplemental Figure 1. QC organization in the roots of *an3*/*gif* mutants.

Supplemental Figure 2. Characterization of *gif2 gif3* and *an3 gif3* roots.

Supplemental Figure 3. *an3-1* root phenotypes.

Supplemental Figure 4. Cell cycle duration in an3/gif mutants.

Supplemental Figure 5. Effects of *an3 gif2* and *Pro35S:miR396* on root meristem size and QC integrity.

Supplemental Figure 6. *ProPLT:CFP* expression in *an3* mutants.

Supplemental Table 1. Quantification of *an3 gif2 AN3-GR* roots with QC defects upon DEX treatment.

Supplemental Table 2. Frequency of QC defects in *an3 brm* crosses.

Supplemental Table 3. Expression of *ProAGL42:GFP* in *an3*/*gif* mutants.

Supplemental Table 4. Mutants and reporter lines used in this study.

Supplemental Table 5. Binary plasmids generated in this study.

Supplemental Table 6. ANOVA tables.

Supplemental Table 7. Locus IDs and oligonucleotide primers used in RT-qPCR.

ACKNOWLEDGMENTS

We thank Ben Scheres for the *ProPLT1:CFP* and *ProPLT2*CFP reporters; Jen Hoe Kim for the *an3*/*gif1*, *gif2*, and *gif3* mutants; Cezary Smaczniak and Kerstin Kauffman for the *BRAHMA* reporter; Yuhai Cui for the *brm-1* mutant; Miguel Moreno-Risueño, Julia Baulies, and Carla Schommer for comments on the manuscript; and Rodrigo Vena, Camila Goldy, and Enrique Morales for help with microscope imaging. M.F.E., J.M.D., A.F., and A.P.P. were supported by fellowships from CONICET. R.E.R. and J.P. are members of CONICET. R.E.R. was supported by ANPCyT (PICT 2012/1686). This work was also supported by grants to J.F.P. (ANPCyT PICT 2015-3557 and 2016-0761).

AUTHOR CONTRIBUTIONS

M.F.E., R.E.R., and J.P. conceived and designed the research. M.F.E., J.M.D., R.E.R., A.F., and A.P. performed the experiments. M.F.E., R.E.R., and J.F.P. analyzed data. M.F.E. and J.P. wrote the manuscript.

Received November 7, 2017; revised January 2, 2018; accepted January 18, 2018; published January 18, 2018.

REFERENCES

Aida, M., Beis, D., Heidstra, R., Willemsen, V., Blilou, I., Galinha, C., Nussaume, L., Noh, Y.S., Amasino, R., and Scheres, B. (2004). The PLETHORA genes mediate patterning of the Arabidopsis root stem cell niche. Cell **119:** 109–120.

Chen, Q., et al. (2011). The basic helix-loop-helix transcription factor MYC2 directly represses PLETHORA expression during jasmonate-mediated modulation of the root stem cell niche in Arabidopsis. Plant Cell **23:** 3335–3352.

Clough, S.J., and Bent, A.F. (1998). Floral dip: a simplified method for Agrobacterium-mediated transformation of *Arabidopsis thaliana*. Plant J. **16:** 735–743.

Cruz-Ramírez, A., Díaz-Triviño, S., Wachsman, G., Du, Y., Arteága-Vázquez, M., Zhang, H., Benjamins, R., Blilou, I., Neef, A.B., Chandler, V., and Scheres, B. (2013). A SCARECROW-RETINOBLASTOMA protein network controls protective quiescence in the Arabidopsis root stem cell organizer. PLoS Biol. **11:** e1001724.

Czechowski, T., Stitt, M., Altmann, T., Udvardi, M.K., and Scheible, W.R. (2005). Genome-wide identification and testing of superior reference genes for transcript normalization in Arabidopsis. Plant Physiol. **139:** 5–17.

Debernardi, J.M., Mecchia, M.A., Vercruyssen, L., Smaczniak, C., Kaufmann, K., Inze, D., Rodriguez, R.E., and Palatnik, J.F. (2014). Post-transcriptional control of GRF transcription factors by microRNA miR396 and GIF co-activator affects leaf size and longevity. Plant J. **79:** 413–426.

Dello Ioio, R., Nakamura, K., Moubayidin, L., Perilli, S., Taniguchi, M., Morita, M.T., Aoyama, T., Costantino, P., and Sabatini, S. (2008). A genetic framework for the control of cell division and differentiation in the root meristem. Science **322:** 1380–1384.

Ercoli, M.F., Rojas, A.M., Debernardi, J.M., Palatnik, J.F., and Rodriguez, R.E. (2016). Control of cell proliferation and elongation by miR396. Plant Signal. Behav. **11:** e1184809.

Fendrych, M., Van Hautegem, T., Van Durme, M., Olvera-Carrillo, Y., Huysmans, M., Karimi, M., Lippens, S., Guérin, C.J., Krebs, M., Schumacher, K., and Nowack, M.K. (2014). Programmed cell death controlled by ANAC033/SOMBRERO determines root cap organ size in Arabidopsis. Curr. Biol. **24:** 931–940.

Galinha, C., Hofhuis, H., Luijten, M., Willemsen, V., Blilou, I., Heidstra, R., and Scheres, B. (2007). PLETHORA proteins as dose-dependent master regulators of Arabidopsis root development. Nature **449:** 1053–1057.

González-García, M.P., Vilarrasa-Blasi, J., Zhiponova, M., Divol, F., Mora-García, S., Russinova, E., and Caño-Delgado, A.I. (2011). Brassinosteroids control meristem size by promoting cell cycle progression in Arabidopsis roots. Development **138:** 849–859.

Heidstra, R., and Sabatini, S. (2014). Plant and animal stem cells: similar yet different. Nat. Rev. Mol. Cell Biol. **15:** 301–312.

Heyman, J., Kumpf, R.P., and De Veylder, L. (2014). A quiescent path to plant longevity. Trends Cell Biol. **24:** 443–448.

Heyman, J., Cools, T., Vandenbussche, F., Heyndrickx, K.S., Van Leene, J., Vercauteren, I., Vanderauwera, S., Vandepoele, K., De Jaeger, G., Van Der Straeten, D., and De Veylder, L. (2013). ERF115 controls root quiescent center cell division and stem cell replenishment. Science **342:** 860–863.

Hiratsu, K., Matsui, K., Koyama, T., and Ohme-Takagi, M. (2003). Dominant repression of target genes by chimeric repressors that include the EAR motif, a repression domain, in Arabidopsis. Plant J. **34:** 733–739.

Horiguchi, G., Kim, G.T., and Tsukaya, H. (2005). The transcription factor AtGRF5 and the transcription coactivator AN3 regulate cell proliferation in leaf primordia of *Arabidopsis thaliana*. Plant J. **43:** 68–78.

Kanei, M., Horiguchi, G., and Tsukaya, H. (2012). Stable establishment of cotyledon identity during embryogenesis in Arabidopsis by ANGUSTIFOLIA3 and HANABA TARANU. Development **139:** 2436–2446.

Kaufmann, K., Muiño, J.M., Østerås, M., Farinelli, L., Krajewski, P., and Angenent, G.C. (2010). Chromatin immunoprecipitation (ChIP) of plant transcription factors followed by sequencing (ChIP-SEQ) or hybridization to whole genome arrays (ChIP-CHIP). Nat. Protoc. **5:** 457–472.

Kim, J.H., and Kende, H. (2004). A transcriptional coactivator, AtGIF1, is involved in regulating leaf growth and morphology in Arabidopsis. Proc. Natl. Acad. Sci. USA **101:** 13374–13379.

Lee, B.H., Wynn, A.N., Franks, R.G., Hwang, Y.S., Lim, J., and Kim, J.H. (2014). The Arabidopsis thaliana GRF-INTERACTING FACTOR gene family plays an essential role in control of male and female reproductive development. Dev. Biol. **386:** 12–24

Livak, K.J., and Schmittgen, T.D. (2001). Analysis of relative gene expression data using real-time quantitative PCR and the 2(-Delta Delta C(T)) method. Methods **25:** 402–408.

Long, Y., Stahl, Y., Weidtkamp-Peters, S., Postma, M., Zhou, W., Goedhart, J., Sánchez-Pérez, M.I., Gadella, T.W.J., Simon, R., Scheres, B., and Blilou, I. (2017). In vivo FRET-FLIM reveals cell-type-specific protein interactions in Arabidopsis roots. Nature **548:** 97–102.

Mähönen, A.P., Ten Tusscher, K., Siligato, R., Smetana, O., Díaz-Triviño, S., Salojärvi, J., Wachsman, G., Prasad, K., Heidstra, R., and Scheres, B. (2014). PLETHORA gradient formation mechanism separates auxin responses. Nature **515:** 125–129.

Mecchia, M.A., Debernardi, J.M., Rodriguez, R.E., Schommer, C., and Palatnik, J.F. (2013). MicroRNA miR396 and RDR6 synergistically regulate leaf development. Mech. Dev. **130:** 2–13.

Moubayidin, L., et al. (2013). Spatial coordination between stem cell activity and cell differentiation in the root meristem. Dev. Cell **26:** 405–415.

Nagai, M., Tanaka, S., Tsuda, M., Endo, S., Kato, H., Sonobe, H., Minami, A., Hiraga, H., Nishihara, H., Sawa, H., and Nagashima, K. (2001). Analysis of transforming activity of human synovial sarcoma-associated chimeric protein SYT-SSX1 bound to chromatin remodeling factor hBRM/hSNF2 alpha. Proc. Natl. Acad. Sci. USA **98:** 3843–3848.

Nawy, T., Lee, J.Y., Colinas, J., Wang, J.Y., Thongrod, S.C., Malamy, J.E., Birnbaum, K., and Benfey, P.N. (2005). Transcriptional profile of the Arabidopsis root quiescent center. Plant Cell **17:** 1908–1925.

Nelissen, H., et al. (2015). Dynamic changes in ANGUSTIFOLIA3 complex composition reveal a growth regulatory mechanism in the maize leaf. Plant Cell **27:** 1605–1619.

O'Malley, R.C., Huang, S.C., Song, L., Lewsey, M.G., Bartlett, A., Nery, J.R., Galli, M., Gallavotti, A., and Ecker, J.R. (2016). Cistrome and epicistrome features shape the regulatory DNA landscape. Cell **166:** 1598.

Ortega-Martínez, O., Pernas, M., Carol, R.J., and Dolan, L. (2007). Ethylene modulates stem cell division in the *Arabidopsis thaliana* root. Science **317:** 507–510.

Perani, M., Ingram, C.J., Cooper, C.S., Garrett, M.D., and Goodwin, G.H. (2003). Conserved SNH domain of the proto-oncoprotein SYT interacts with components of the human chromatin remodelling complexes, while the QPGY repeat domain forms homo-oligomers. Oncogene **22:** 8156–8167.

Petricka, J.J., Winter, C.M., and Benfey, P.N. (2012a). Control of Arabidopsis root development. Annu. Rev. Plant Biol. **63:** 563–590.

Petricka, J.J., Schauer, M.A., Megraw, M., Breakfield, N.W., Thompson, J.W., Georgiev, S., Soderblom, E.J., Ohler, U., Moseley, M.A., Grossniklaus, U., and Benfey, P.N. (2012b). The protein expression landscape of the Arabidopsis root. Proc. Natl. Acad. Sci. USA **109:** 6811–6818.

Rodriguez, R.E., Schommer, C., and Palatnik, J.F. (2016). Control of cell proliferation by microRNAs in plants. Curr. Opin. Plant Biol. **34:** 68–76.

Rodriguez, R.E., Mecchia, M.A., Debernardi, J.M., Schommer, C., Weigel, D., and Palatnik, J.F. (2010). Control of cell proliferation in *Arabidopsis thaliana* by microRNA miR396. Development **137:** 103–112.

Rodriguez, R.E., Ercoli, M.F., Debernardi, J.M., Breakfield, N.W., Mecchia, M.A., Sabatini, M., Cools, T., De Veylder, L., Benfey, P.N., and Palatnik, J.F. (2015). MicroRNA miR396 regulates the switch between stem cells and transit-amplifying cells in Arabidopsis roots. Plant Cell **27:** 3354–3366.

Sabatini, S., Heidstra, R., Wildwater, M., and Scheres, B. (2003). SCARECROW is involved in positioning the stem cell niche in the Arabidopsis root meristem. Genes Dev. **17:** 354–358.

Sang, Y., Silva-Ortega, C.O., Wu, S., Yamaguchi, N., Wu, M.F., Pfluger, J., Gillmor, C.S., Gallagher, K.L., and Wagner, D. (2012). Mutations in two non-canonical Arabidopsis SWI2/SNF2 chromatin remodeling ATPases cause embryogenesis and stem cell maintenance defects. Plant J. **72:** 1000–1014.

Santuari, L., et al. (2016). The PLETHORA gene regulatory network guides growth and cell differentiation in Arabidopsis roots. Plant Cell **28:** 2937–2951.

Sarkar, A.K., Luijten, M., Miyashima, S., Lenhard, M., Hashimoto, T., Nakajima, K., Scheres, B., Heidstra, R., and Laux, T. (2007). Conserved factors regulate signalling in *Arabidopsis thaliana* shoot and root stem cell organizers. Nature **446:** 811–814.

Scheres, B. (2007). Stem-cell niches: nursery rhymes across kingdoms. Nat. Rev. Mol. Cell Biol. **8:** 345–354.

Schindelin, J., et al. (2012). Fiji: an open-source platform for biological-image analysis. Nat. Methods **9:** 676–682.

Smaczniak, C., et al. (2012). Characterization of MADS-domain transcription factor complexes in Arabidopsis flower development. Proc. Natl. Acad. Sci. USA **109:** 1560–1565.

Vanstraelen, M., Baloban, M., Da Ines, O., Cultrone, A., Lammens, T., Boudolf, V., Brown, S.C., De Veylder, L., Mergaert, P., and Kondorosi, E. (2009). APC/C-CCS52A complexes control meristem maintenance in the Arabidopsis root. Proc. Natl. Acad. Sci. USA **106:** 11806–11811.

Vercruyssen, L., et al. (2014). ANGUSTIFOLIA3 binds to SWI/SNF chromatin remodeling complexes to regulate transcription during Arabidopsis leaf development. Plant Cell **26:** 210–229.

Vilarrasa-Blasi, J., González-García, M.P., Frigola, D., Fàbregas, N., Alexiou, K.G., López-Bigas, N., Rivas, S., Jauneau, A., Lohmann, J.U., Benfey, P.N., Ibañes, M., and Caño-Delgado, A.I. (2014). Regulation of plant stem cell quiescence by a brassinosteroid signaling module. Dev. Cell **30:** 36–47.

Yang, S., Li, C., Zhao, L., Gao, S., Lu, J., Zhao, M., Chen, C.Y., Liu, X., Luo, M., Cui, Y., Yang, C., and Wu, K. (2015). The Arabidopsis SWI2/SNF2 chromatin remodeling ATPase BRAHMA targets directly to PINs and is required for root stem cell niche maintenance. Plant Cell **27:** 1670–1680.